Chapter 5

Modeling Dynamic-Weakening and Dynamic-Strengthening of Granite in High-Velocity Slip Experiments

Zonghu Liao and Ze'ev Reches

Additional information is available at the end of the chapter

http://dx.doi.org/10.5772/54889

1. Introduction

Earthquakes are associated with slip along fault-zones in the crust, and the intensity of dynamic-weakening is one of the central questions of earthquake physics (Dieterich, 1979; Reches and Lockner, 2010). Since it is impossible to determine fault friction with seismological methods (Kanamori and Brodsky, 2004), the study of fault friction and earthquake weakening has been usually addressed with laboratory experiments (Dieterich, 1979) and theoretical models (Ohnaka and Yamashita, 1989).

The experimental analyses of dynamic-weakening were conducted in several experimental configurations: bi-axial direct shear (Dieterich, 1979; Samuelson et al, 2009), tri-axial confined shear (Lockner and Beeler, 2002), and rotary shear apparatus (Tsutsumi and Shimamoto, 1997; Goldsby and Tullis, 2002; Di Toro et al., 2004; Reches and Lockner, 2010). The direct shear apparatus allows high normal stress and controlled pore water pressure (up to ~200 MPa) with limited slip velocity (up to 0.01 m/s) and limited slip distance (~10 mm) (Shimamoto and Logan, 1984). These slip velocities and displacements are significantly smaller than those of typical earthquakes (0.1-10 m/s and up to 5 m, respectively). In order to study high velocity and long slip distance, experiments have been conducted in rotary shear machines.

While many studies indicated a systematic weakening with increasing slip-velocity (Dieterich, 1979; Di Toro et al., 2011), recent experimental observations revealed an opposite trend of dynamic-strengthening particularly under high velocity (Reches and Lockner, 2010; Kuwano and Hatano, 2011). This strengthening was attributed to dehydration of the fault gouge due to frictional heating at elevated velocities (Reches and Lockner, 2010; Sammis et al., 2011). If

similar dynamic-strengthening occurs during earthquakes, it should be incorporated in the analyses of earthquake slip.

We analyze here of the relations between friction coefficient and slip velocity for steady-state velocity the range of 0.001-1 m/s. These relations are derived for the Sierra White granite (SWG) experiments under normal stress up to 7 MPa. The results are presented by a model that is termed WEST (WEkening-STrengtheing). We first present the main experiment observations, for five rock types, and then we derive the numeric model for Sierra White granite (SWG). Finally, we apply the numerical model to tens of experiments with complex velocity history conducted on the same rock.

2. Experimental observations

The experiments were conducted with a rotary shear apparatus and cylindrical rock samples (Reches and Lockner, 2010; Chang et al., 2012). The experimental setup and sample configuration are described in Appendix A. The experimentally monitored parameters include slip distance, slip velocity, fault-normal displacement (dilation), shear stress and normal stress. Sample temperature was measured by thermocouples that are embdded ~3mm away from the slip surfaces. The normal load was maintained constant during a given experiment, and the experiments were performed at room conditions. Fault strength is represented by the friction coefficient, $\mu = \tau/\sigma_N$ (where τ is shear stress and σ_N the normal stress). The slip velocity was either maintained constant, or increased or decreased in steps. We present results of tests with samples of Sierra White granite (after Reches and Lockner, 2010), and new results for samples of Blue quartzite, St. Cloud diorite, Fredricksburg syenite, and Karoo gabbro. The tests with SWG samples were run under the widest range of conditions and the numeric model was derived only for this rock.

Reches and Lockner (2010) determined the friction-velocity relations of SWG for a velocity range of.0003-1 m/s and normal stress up to 7 MPa. Their results revealed three general regimes of friction-velocity relations (Fig. 1a):

i. Dynamic-weakening (drop of 20-60% of static strength) as slip velocity increased from ~0.0003 m/s to a critical velocity of V_c ~ 0.03 m/s, during which the friction coefficient was 0.3-0.45.

ii. Transition to dynamic-strengthening regime in the velocity range of V = 0.06-0.2 m/s, during which the fault strength almost regained its static strength; and

iii. Quasi-constant strength for V > 0.2 m/s, with possible further drops as velocity approaches ~1 m/s. Only few experiments were conducted in this range due to sample failure by thermal fracturing.

Similar pattern of weakening-strengthening of Westerly granite samples was recently observed by Kuwano and Hatano (2011) (Fig. 1b). They showed that the friction coefficient dropped in the velocity range of 0.001-0.06 m/s, and rose in the velocity range of 0.06-0.2 m/s

http://dx.doi.org/10.5772/54889

(Fig. 1b). Earlier work of Tsutsumi and Shimamoto (1997) also indicated temporal periods of strengthening, in which the friction sharply increased, and visible melting was observed at the strength peak when the slip rate was increased from 0.55 to 0.73 m/s.

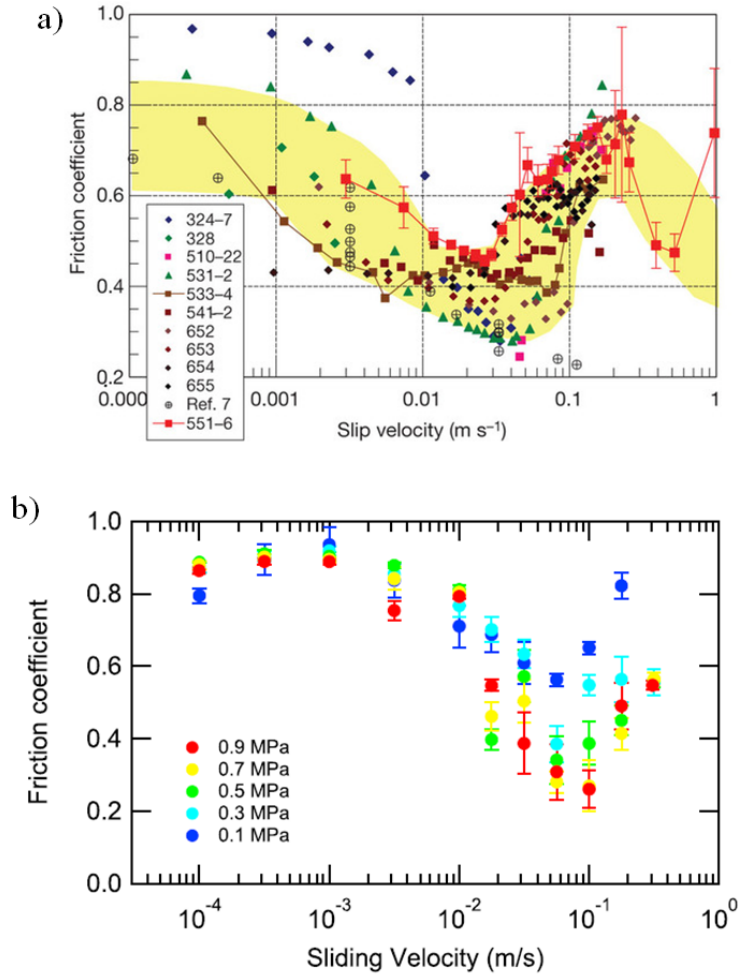

Figure 1. Experimental friction-velocity relations in (a) Sierra White granite (after Reches and Lockner, 2010) and (b) Westerly ganite (after Kuwano and Hatano, 2011

To further explore the occurrence of dynamic-strengthening, we tested four other rocks under conditions similar to Reches and Lockner (2010) tests. The new experiments were conducted on samples made of Blue quartzite (Fig. 2a), St. Cloud diorite (Fig. 2b), Fredricksburg syenite (Fig. 2c), and Karoo gabbro (Fig. 2d). The diorite (Fig. 2b) and syenite (Fig. 2c) samples

displayed a distinct transition into dynamic-strengthening regime (red arrows). The critical transition velocity, V_C, depends on the sample lithology; it is ~0.02 m/s and ~0.01 m/s for the diorite and syenite, respectively. The Blue quartzite tests displayed only negligible weakening and strengthening (Fig. 2a).

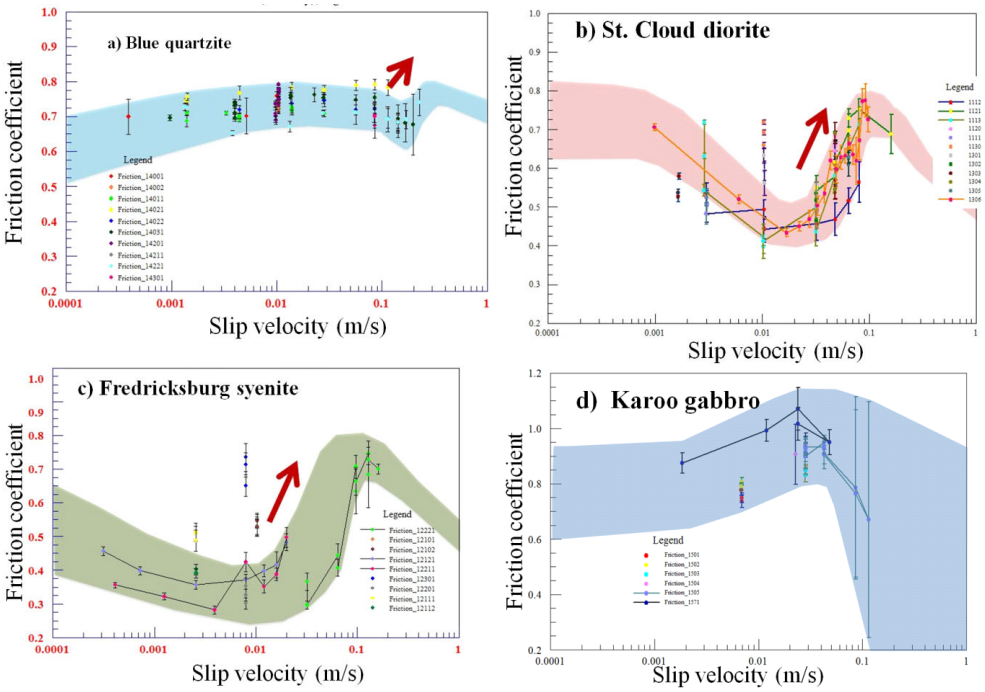

Figure 2. Friction-velocity relations in shear experiements of Blue quartzite (a), St. Cloud diorite (b), Fredricksburg syenite (c), and Karoo gabbro (d). Connected lines indicated data from step-velocities experiments. Unconnected dots indicate single velocity experiments.Note velocity-weakening and velocity-strengthening stages (marked by red arrows) in (a)-(c) and no velocity-strengthening in (d).

3. Numerical modeling

3.1. Approach

The most striking feature of the relations between the friction coefficient and slip-velocity for the above experiments is the systematic transition from weakening under low velocity to strengthening at higher velocities (Figs. 1, 2). We refer to this feature of **WE**akening-**ST**rengthening as the **WEST** mode, and developed a numerical model to describe its character. The model is based on two central assumptions. First, the friction coefficients, in both weakening and strengthening regimes, can be presented as dependent of the slip distance, and slip

http://dx.doi.org/10.5772/54889

velocity. This assumption was employed in many previous models (Dieterich, 1979; Beeler et al, 1994; Tsutsumi and Shimamoto, 1997; Reches and Lockner, 2010; Di Toro et al., 2011). Second, the weakening-strengthening mode reflects a transition between different frictional mechanisms. Reches and Lockner (2010) and Sammis et al. (2011) suggested that the weakening is controlled by gouge powder lubrication due to coating of the powder grains by a thin layer of water that is 2-3 monolayers thick. The dehydration of this layer at elevated temperature under high slip velocity leads to strengthening. It is thus assumed that the weakening and strengthening regimes have different parametric relation between friction and velocity.

3.2. Model formulation

Following the above assumptions, we model the relations of the steady-state friction coefficient, μ, and the slip distance, D, and slip-velocity, V (Fig. 3). The steady-state is defined for a given slip velocity during which the weakening (or strengthening) intensifies with increasing slip distance. The model addresses the three major features of the experimental observation: (I) the slip-weakening relation, μ(V, D), represents the drop from static friction coefficient, μ_S, to the kinematic friction coefficient, μ_K during slip to the critical distance, D_C, at a constant velocity; (II) the dynamic-friction coefficient, $\mu_K(V)$, at $V < V_C$, under steady-state; and (III) the dynamic-strengthening at high velocity regime of $V > V_C$. We regard the friction coefficient decrease from (1) to (2) (Fig. 3) as the dynamic-weakening, and the friction coefficient increase from (2) to (3) as dynamic-strengthening.

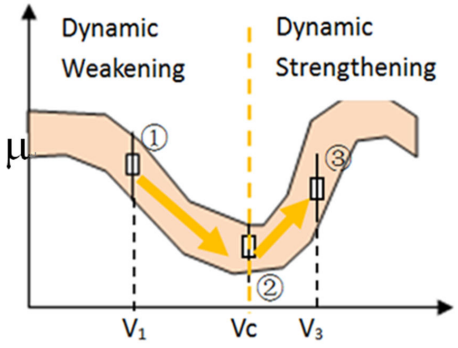

Figure 3. A schematic presentation of WEST model, with velocity controlled kinematic friction coeefcient.

The dependence of the experimentally monitored friction coefficient, μ, on the two experimentally controlling factors of D and V has the general form of

$$\mu = \mu(D, V) \tag{1}$$

The friction coefficient, μ, has two end members, the static friction coefficient, μ_S, which is the friction coefficient during slip initiation, and the kinematic friction coefficient, μ_K, the steady-

state coefficient after large slip distance under a constant velocity. The transition between the weakening regime and the strengthening regime occurs at the critical slip-velocity, $\mathbf{V_C}$, that is determined from the general plot of friction coefficient as function of slip-velocity (Fig. 1, 2, 3).

We assume that during the weakening stage and under constant velocity, the drop of μ from $\boldsymbol{\mu_S}$ to $\boldsymbol{\mu_K}$ is controlled only by the slip distance D,

$$\mu = \mu(D), when \boldsymbol{\mu_S} > \mu > \boldsymbol{\mu_K}, \tag{2}$$

where,

$$\begin{aligned} &\mu = \boldsymbol{\mu_S} \; for \; V = 0 \; and \; D = 0 \; (Slip \; initiation), && \text{a} \\ &\text{and} \\ &\mu = \boldsymbol{\mu_K} \; for \; steady-state \; velocity, \; V, \; and \; D > D_C, && \text{b} \end{aligned} \tag{3}$$

where D_C is the critical slip distance.

It is also assumed that $\boldsymbol{\mu_K}$ is a function only of slip velocity V,

$$\boldsymbol{\mu_K} = \boldsymbol{\mu_K}(V), \tag{4}$$

Similarly, we assume that during the strengthening stage, μ is a function of both slip-velocity and slip distance,

$$\mu = \mu(D, V), for \; V > V_{C,} \tag{5}$$

This approach for the empirical relations is in the spirit of the weakening relations developed by Dieterich (1979) who introduced the rate- and state- friction law.

3.3. Model parameterization

General

Solutions for the model functional relations were searched in the following steps.

1. Prepare a table of the experimental velocity-friction relation;
2. Select experiments with representative weakening stage;
3. Search for a suitable functional fit between slip velocities, friction coefficient, and slip distance. For this search, we chose the simplest functional relation that provided good fit. The search revealed the relations between the $\boldsymbol{\mu_K}$ and velocity.
4. Integrate the above relations for the effect of distance and velocity.

http://dx.doi.org/10.5772/54889

5. Apply the above functional relations to set up the specific WEST model (Equations 2, 4, 5).

Dynamic-weakening regime

The experimental data set has large data scatter at low velocities (Fig.1; Reches and Lockner, 2010). For the range of V < 0.03 m/s (Fig. 4), we found the following relations of μ_K and slip velocity,

$$\mu_K(V) = 0.742 - \frac{0.375V}{0.00183 + V}, \quad \text{for } V \leq 0.03 \text{ m/s} \tag{6}$$

The RMS (root mean square) of this solution is 0.83 while the correlation coefficient is 0.73. This simple solution provides reasonable fit to the scattered friction data (Fig. 4).

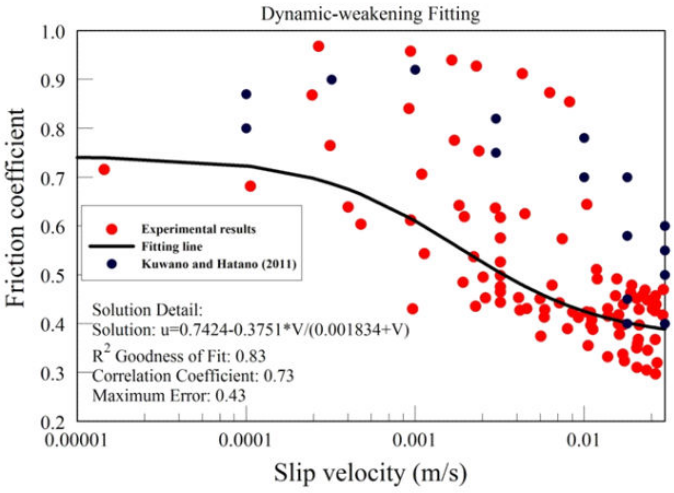

Figure 4. The selected solution (red curve) for dynamic-weakening of kinetic friction coefficient of SWG for V = 0.0003-0.03m/s by Eureqa. Data for V < 0.003 m/s are from Reches and Lockner (2010) and Kuwano and Hatano (2011).

Dynamic-strengthening regime

In the strengthening regime of 0.03 m/s < V < 1.0 m/s (Fig. 5), the selected solution for velocity-controlled friction coefficient is

$$\mu_K(V) = 0.824 \exp\left(-\frac{0.0275}{V}\right) \text{for } V > 0.03 m/s \tag{7}$$

The RMS of this solution is 0.91 and the correlation coefficient is 0.74. The trend of this exponential relation provide good fit for SWG (Reches and Lockner, 2010) in the strengthening trend (Fig. 5), and this trend generally fit the experimental results of Kuwano and Hatano (2011). Note: Friction during 0.305-0.4 m has been locally adjusted to comply with Fig. 4.

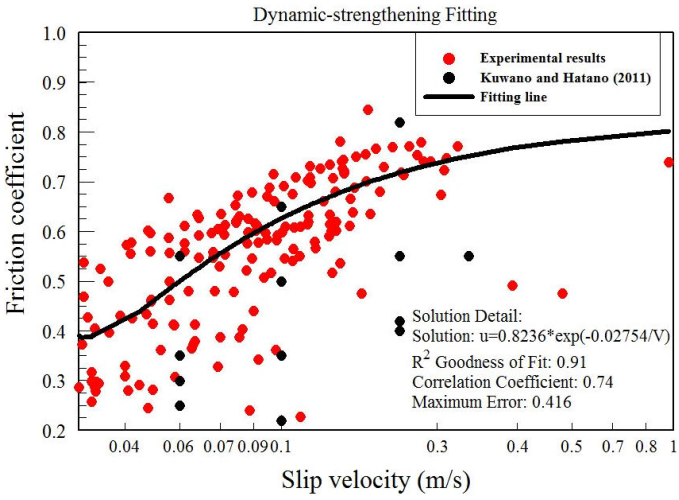

Figure 5. a) The selected solution (red curve) for dynamic-strengthening of SWG for V = 0.03-0.3m/s by Eureqa. Data for V > 0.003 m/s are from Reches and Lockner (2010) and Kuwano and Hatano (2011)

Slip-weakening relations

For the ten experimental results (Fig. 6), we selected the slip-weakening function as,

$$\mu = \mu(D) = 0.2663\ (\pm 0.1)\exp(-D) + 0.4061(\pm 0.15) \tag{8}$$

For D=0, which is slip initiation, the calculated $\mu = \mu_S = 0.6724$. For D > Dc (e.g., 3.0 m), the calculated $\mu = \mu_K = 0.41$.

http://dx.doi.org/10.5772/54889

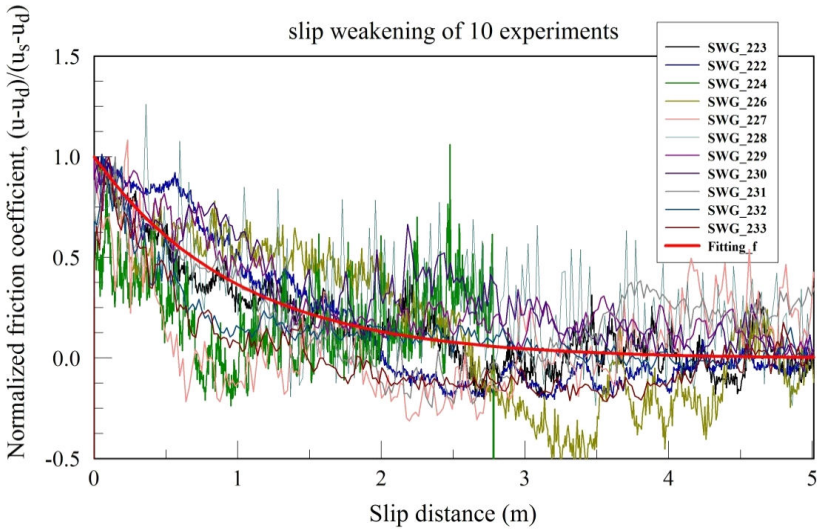

Figure 6. a) The best fit solution (red curve) for slip distance weakening in ten experiments. SWG 222, 223, 224 were run at velocity 0.024 m/s; SWG 226-232 were run at 0.072 m/s; σ_N = 1.1 MPa. The solution is μ= 0.2663(±0.1) exp (-D) +0.4061(±0.15). The constants can be adjusted for specific case

Model synthesis

By substitute the 0.4061 (Eq. 8) by Eq. (7), Eq. (8) is generalized into,

$$\mu(D, V) = 0.2663 \bullet \exp(-D) + \mu_K(V) \tag{9}$$

which combines Eq. (2, 4, 5). This simple exponential function characterized the weakening process with relating small deviation of the data. A summary of WEST equations is listed in Table 1.

Terms	Expression	Eq. Number
General function	$\mu = \mu(D, V)$	(1)
Slip-weakening	$\mu(D, V) = 0.2663 \exp(-D) + \mu_K(V)$	(9)
Dynamic-weakening	$\mu_K(V) = 0.742 - \frac{0.375V}{0.00183 + V}$, for $V \le 0.03$ m / s	(6)
Dynamic-strengthening	$\mu_K(V) = 0.824 \exp\left(-\frac{0.0275}{V}\right)$, for $V > 0.03 m/s$	(7)

Table 1. A summary of WEST equations.

4. Model application and analysis

4.1. General

We now apply the WEST model to simulate the friction-velocity-distance evolution in a set of experiments with Sierra White granite. In these simulations, we use the experimental slip distance, D, and slip velocity, V, which were controlled by the operator, as input parameters in Equations (6, 7, 9) and Table 1. This substitution predicts the evolution of the friction coefficient during the experiments. The predicted friction coefficient is then plotted with the experimentally observed equivalent. The simulations were done on four types of velocity histories; none of the simulated experiment was used for the derivation of the model.

4.2. Rising velocity steps

We start with three runs under same σ_N = 5.0MPa, and each with three upward stepping velocities, 0.0025, 0.025 and 0.047 m/s. During these runs the cumulative slip was about 9 m (Fig. 7). These velocities are in the weakening regime, and they display intense friction drops that reflect both the rising velocity and increase of slip distance. The friction coefficient was 0.7-0.9 at the first step of V = 0.0025 m/s, and it decreased to $\mu \cong 0.5$ in the second velocity step of V = 0.025 m/s. A minimum of friction coefficient of μ = 0.4 developed under V = 0.05 m/s. This experimental evolution fits well the predictions by WEST model.

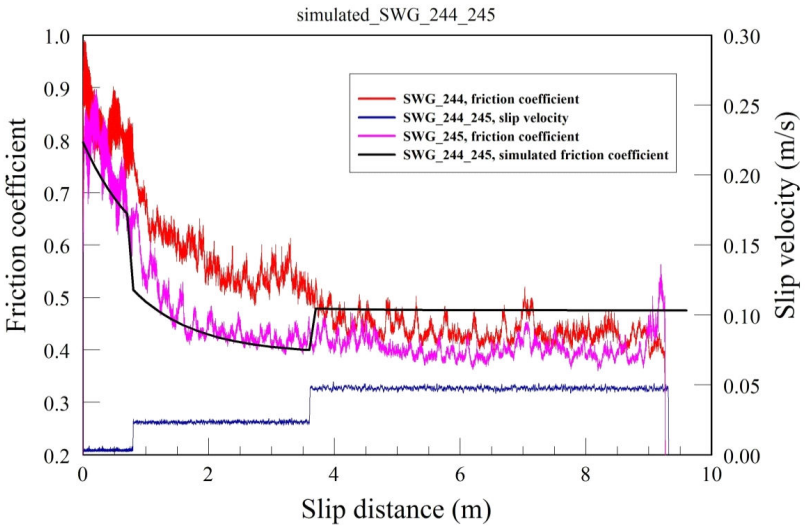

Figure 7. WEST model simulation and experimental results for SWG experiments 244, 245, SWG, σ_N = 5.0 MPa

http://dx.doi.org/10.5772/54889

4.3. Rise and drop

We now examine two groups of experiments, each with five runs of the same loading conditions (σ_N = 5.0MPa). Each group has three velocity stages: low, high, and back to low. In the first group, the three steps were 0.00075, 0.0075, and 0.00075 m/s. The initial friction coefficient ranged 0.4-0.7 for the different runs in the group, and during the first step, the friction coefficient was gradually decreased by ~0.1. During the second stage of V = 0.0075 m/s, which lasted 10 s, the friction coefficient reduced drastically, with larger reduction of the runs that started at higher friction coefficient. During the final, low velocity, the sample was slightly strengthened.

In Fig. 8, this group of experiments was performed on the same sample under σ_N = 5.0MPa. The different initial friction coefficients (e.g., runs 1, 2 have higher friction coefficient than run 3, 4, 5) were attributed to the holding-times between experiments. The weakening was well noticed when slip velocity was raised and then the friction reached a relative steady value. The fit line shows the weakening immediately after the velocity has been raised. When the velocity drops, the friction coefficient is raised higher in the fit line than the data.

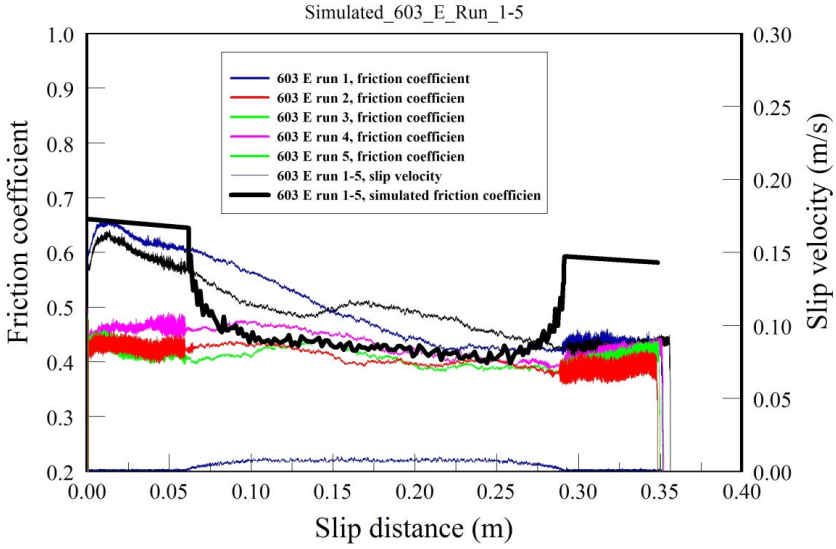

Figure 8. WEST model simulation and experimental results for SWG_603_Run_(1-5), SWG, σN = 5.0 MPa

In the second group (Fig. 9), the scenario was repeated but at velocities which were higher by an order of magnitude: 0.0075 m/s (first and last stages) and 0.075 m/s (second stage). This time, the friction coefficient in the second stage was increased from μ=~0.3 to the highest μ = 0.7. Then, μ gradually reduced to 0.3-0.4 during the final, low velocity stage. In Fig. 9, the friction coefficient of the fit results rises and drops earlier than the experimental data (running from 0.25 m to 0.75 m). The rest of the running, at the beginning low velocity and the final velocity, the friction coefficient between the model and experiments fit well each other.

Comparing the two groups, the different friction responses provide clear evidence for dynamic-strengthening at slip velocity ~ 0.07 m/s.

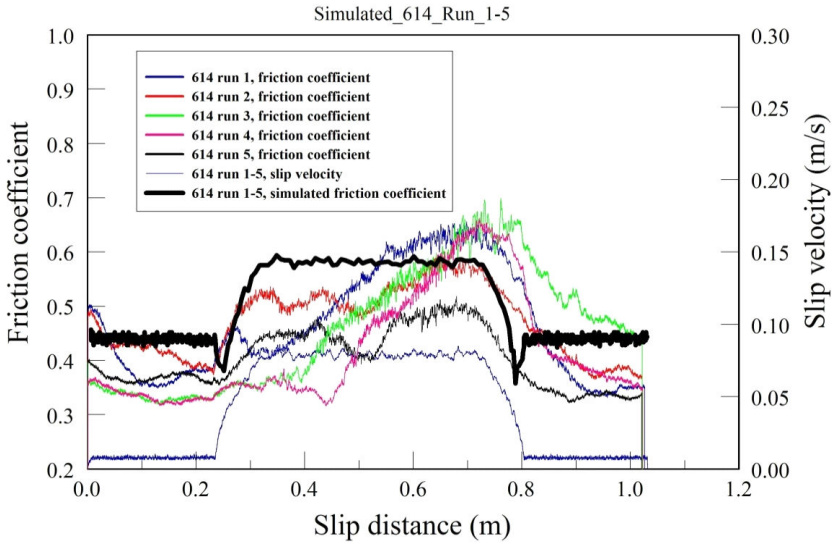

Figure 9. WEST model simulation and experimental results for SWG_614_Run_(1-5), SWG, σ_N = 5.0 MPa

The WEST simulations were also performed to investigate if the model can capture the dynamic-strengthening at the high velocity regime. Fig. 10 is an experiment with five alternating steps of velocity that again indicates the dynamic-strengthening at velocity 0.075 m/s (above the critical value V_C). The friction coefficient dropped from 0.7 to 0.5 at velocity of 0.0025 m/s and 0.025 m/s, then dynamically-strengthened to $\mu = 0.7$ at $V = 0.75$ m/s, and finally slightly dropped to 0.55 with a slip distance of ~4.2 m (from 1.7 m to ~5.9 m) as the velocity decreased. Similarly to the case of rise-drop experiment (Fig. 8), the observed friction coefficient changed only slightly in the end at dropping velocity (from 5.9 m to 7.6 m). The simulation illustrates the dynamic-strengthening during the three-step sliding.

4.4. Drop and rise during long distance slip experiments

In Fig. 11, the simulation presents the experiment behavior that involved three steps: an initial weakening at the higher slip velocity of 0.045 m/s, regaining strengthen at a lower speed of 0.0018 m/s, and a final weakening at high-speed step of 0.045 m/s after healing for about 2,000 seconds. The healing refers to the regaining of strength of the fault during hold time. During the simulation of the second step, the friction coefficient was manually shifted to static value due to healing (indicated by blue arrow, Fig. 11). The increase of friction here is related to healing during hold time, which differs from dynamic-strengthening. The simulation results show smooth lines instead of noisy curves of the experiment.

http://dx.doi.org/10.5772/54889

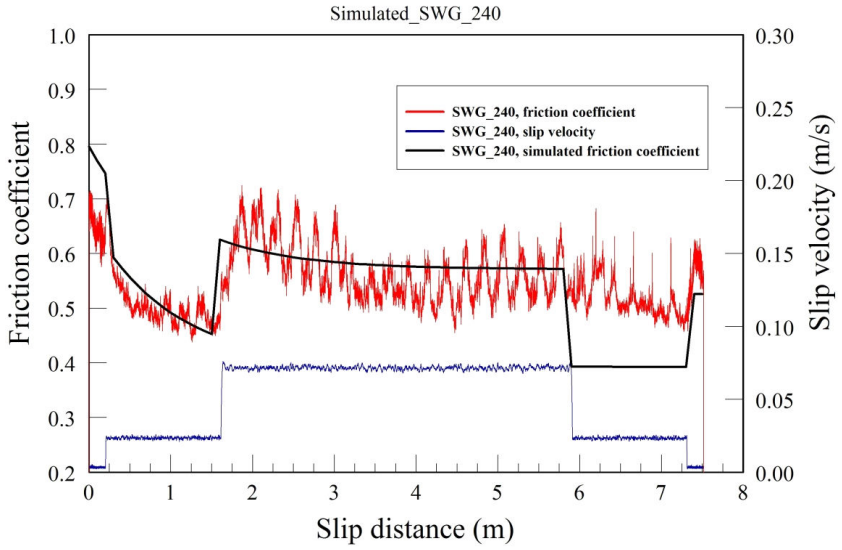

Figure 10. WEST model simulation and experimental results for SWG 240, SWG, σ_N = 1.1 MPa

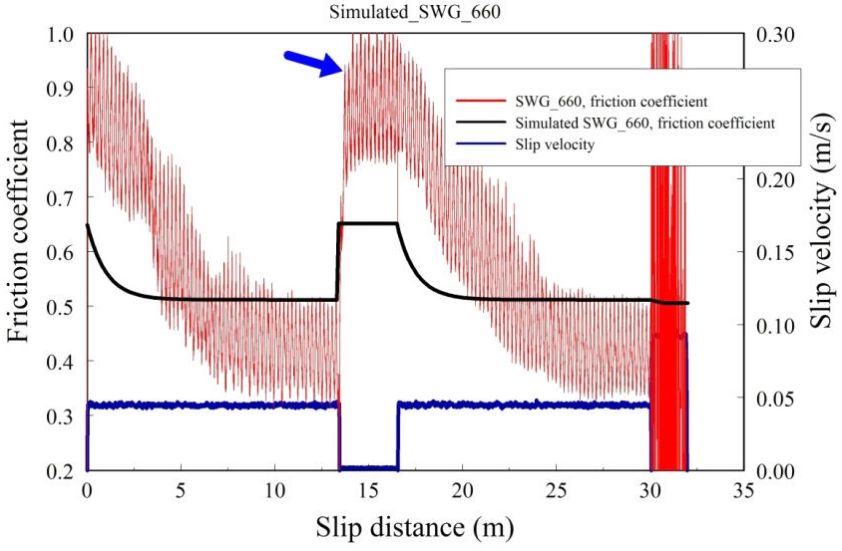

Figure 11. WEST model simulation and experimental results for SWG 660, SWG, σ_N = 0.5MPa. The rising of friction coefficient indicated by blue arrow is NOT dynamic-strengthening

4.5. Wide velocity range

Figs. 12 and 13 display the friction evolution in two experiments with wide velocity range. Fig. 12 displays a slide-hold-slide run under σ_N = 1.1 MPa and hold times of 10 s between the multiple velocity steps. Under this short hold time, the friction coefficient curve displays quasi-continuous trend. There is a marked weakening as the velocity was increased to ~ 0.04 m/s, followed by a gentle strengthening at higher velocities. The modeling results were lower at beginning than expected and strengthening occurred earlier. Fig. 13 displays two major features: an initial gradual weakening in the slip velocity range of ~0.0003 m/s to a critical velocity of ~0.03 m/s, and a fast strengthening at velocities from ~0.03 m/s to 0.2 m/s. In the final stage, the friction reaches ~0.8. The modeling simulates the weakening-strengthening pattern, but it fails to follow the experimental results in the region faster than the critical velocity. In the experiment, the friction coefficient remained relatively low from ~3 m to ~11 m, where the simulated results predicted earlier strengthening. Also, an abrupt friction rise was observed in the experiment (at ~ 11 m) whereas the model indicated smooth and continuous strengthening.

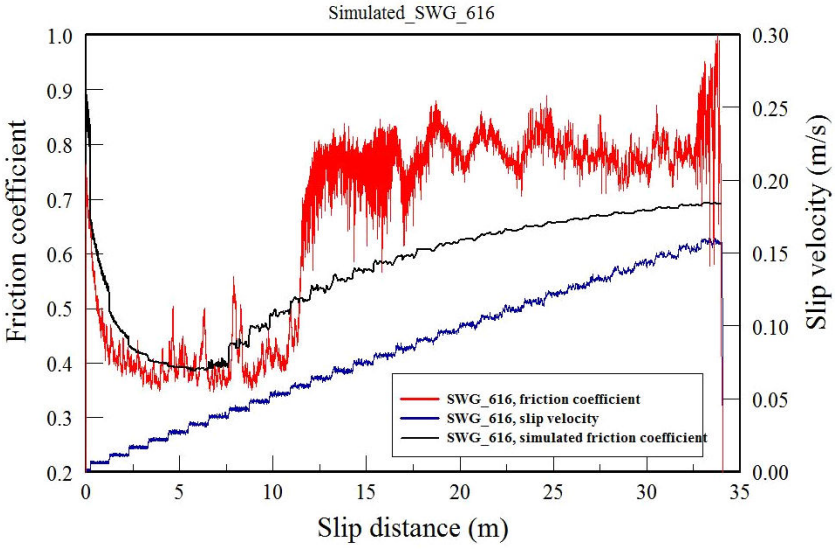

Figure 12. WEST model simulation and experimental results for SWG 531, SWG, σ_N = 1.1MPa. Friction coefficient is shown for a full-velocity by interval holding in sliding distance together with a best fit modeling result

http://dx.doi.org/10.5772/54889

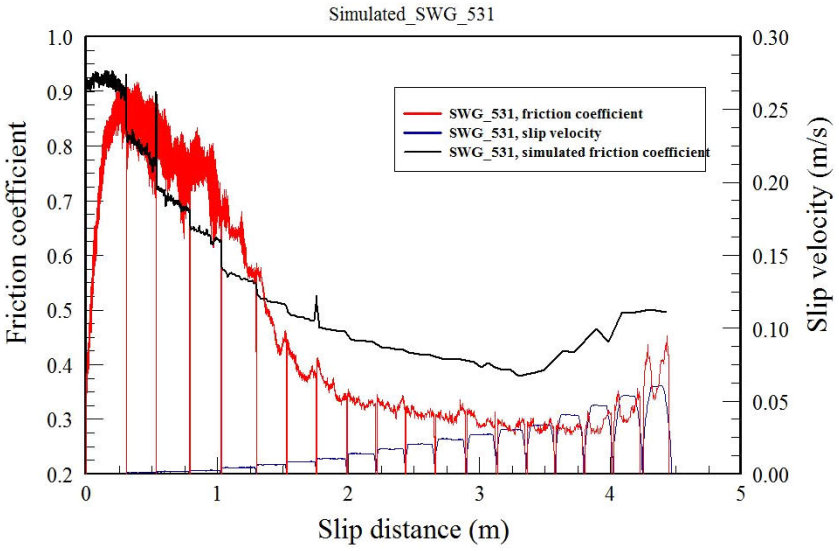

Figure 13. WEST model simulation and experimental results for SWG 616, SWG, σ_N = 5.0 MPa. Friction coefficient is shown for a full-velocity continuously in sliding distance together with a best fit modeling result

5. Discussion

5.1. Field applications

The WEST model was developed for the experimental results of Sierra White granite for which we have multiple runs that well bound the solutions and simulations. The WEST relations (Eqn. 6, 7, 9) represent the empirical frictional history of SWG in the slip-velocity range of 10^{-4}-1m/s. The application of the model to the experimental results shows that friction history can be captured by a numerical combination of the slip velocity and slip distance for both the weakening and strengthening stages. Specifically, in the dynamic-strengthening regime has the following properties: 1) It is a high-velocity regime, $V > V_C$, e.g. V ~ 0.03-0.6 m/s for Sierra White granite; 2) The WEST model uses a kinematic friction coefficient for the strengthening stage, which is derived independently of the weakening stage; 3) The friction coefficient history is well simulated by combining the kinematic friction coefficient for strengthening and the slip distance.

The WEST model predicts the rate-dependence of friction over the full range of observed natural seismic slip-rates, and in this sense it is applicable to earthquake simulations, and modeling of earthquake ruptures. Accumulating evidence supports the presence of dynamic-strengthening. Kaneko et al (2008) stated that "the velocity-strengthening region suppresses supershear propagation at the free surface occurring in the absence of such region, which could

explain the lack of universally observed supershear rupture near the free surface". Hence, it is important to understand how the dynamic friction at seismic rates affects earthquake rupture dynamics by adopting new friction model in the numerical simulations. Although this is beyond the scope of the present study, the abundance of efforts on experimental studies on dynamic friction provides a realistic velocity-friction relation to explore the ground motions during earthquake rupture.

6. Summary

The analysis examines the frictional strength of igneous rocks including granite, diorite, syenite, gabbro, and quartzite under slip-velocity approaching seismic-rates. The experimental observations confirm that increasing slip velocity leads to dynamic-weakening followed by **dynamic-strengthening** only in igneous rock samples that contain quartz (Figs. 1, 2). The weakening-strengthening transition occurs at a critical velocity, V_C, which depends on the fault lithology (Figs. 1, 2).

The present study provides a numerical framework for the experimental observations of dynamic-strengthening at high velocity along rock faults. The model is empirical in nature, and it succeeds to simulate the friction coefficient history in a wide range of experimental loading. We envision that it is a promising tool to analyze rock friction during earthquakes. In future research, several aspects of the sliding mechanism should be linked and interpreted in terms of the WEST model: 1) Powder lubrication by Reches and Lockner (2010) showed that the newly formed gouge organizes itself into a thin deforming layer that changes the fault strength; 2) Fault-strengthening during hold time; and 3) Predicting the effect of lithological compositions on the frictional resistance (Di Toro et al., 2004).

Appendix A: Experiment setup

The analyzed experiments were conducted on the ROGA in University of Oklahoma. The following description of the apparatus is taken from Reches and Lockner (2010) and related lab proposals. The ROGA system (Rotary Gouge Apparatus, Fig. 14) satisfies the following conditions: (1) normal stress of tens to hundreds of MPa; (2) slip velocity of ~1 m/s; (3) rise-time of less than 1 s; and (4) unlimited slip distances.

In the experiments, the fault is composed of solid blocks of Sierra White granite. Each sample includes two cylindrical blocks, diameter = 101.6 mm, height = 50.8 mm. For ~uniform velocity, the upper block has a raised ring with ID = 63.2 mm and OD = 82.3 mm; the blocks are pressed across this raised ring. Thermocouples are cemented into holes drilled 3 mm and 6 mm away from the sliding surfaces (Fig. 14). Each pair of blocks wore to form gouge in between at different slip velocities of 0.001-1 m/s. A large set of experiments will be executed and a large quantity of data will be collected by LabView at frequency of ~100-1000 Hz.

http://dx.doi.org/10.5772/54889

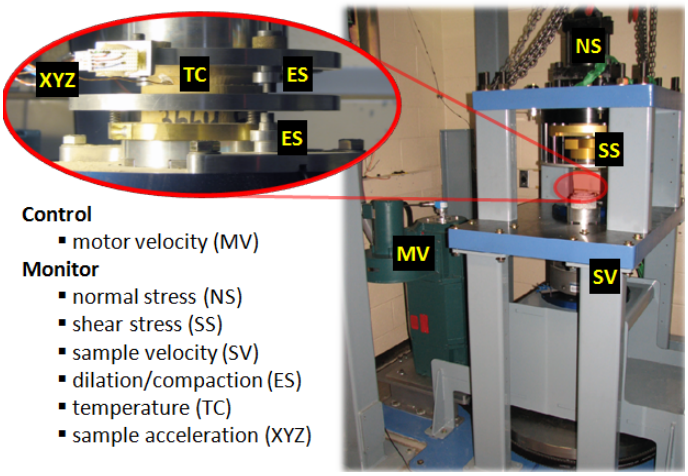

Figure 14. The Rotary Shear Apparatus with builder Joel Young. The sample block assembled in the loading frame (after Reches and Lockner (2010)

Acknowledgements

Discussions and suggestions by David Lockner and Yuval Boneh contributed to the analysis. Usage of the 'Eureqa Formulize' program helped in the model computation. Partial funding support was provided by grants 1045414 of NSF Geosciences, Geophysics, G11AP20008 of DOI-USG-NEHRP2011, and SCEC 2012.

Author details

Zonghu Liao and Ze'ev Reches

School of Geology and Geophysics, University of Oklahoma, Norman, USA

References

[1] Beeler, N. M., T. E. Tullis, and J. D. Weeks (1994), The roles of time and displacement in the evolution effect in rock friction, *Geophys. Res. Lett.*, 21(18), 1987-1990.

[2] Boneh, Y. (2012), Wear and gouge along faults: experimental and mechanical analysis, M.S. thesis, Dep. of Geol. and Geophys., Univ. of Oklahoma, Norman, OK, USA.

[3] Chang, J. C., Lockner, D. A., and Z. Reches (2012), Rapid acceleration leads to rapid weakening in earthquake-like laboratory experiments, *Science*, 338(6103), 101-105.

[4] Di Toro, G., D. L. Goldsby DL, and T. E. Tullis (2004), Friction falls towards zero in quartz rock as slip velocity approaches seismic rates, *Nature*, 427, 436-439.

[5] Di Toro, G., R. Han, T. Hirose, N. De Paola, S. Nielsen, K. Mizoguchi, F. Ferri, M. Cocco, and T. Shimamoto (2011), Fault lubrication during earthquakes, *Nature*, 471, 494-498.

[6] Dieterich, J. H. (1979), Modeling of rock friction: 1. Experimental results and constitutive equations, *J. Geophys. Res*., 84(5), 2161-2168.

[7] Goldsby, D. L., and T. E. Tullis (2003), Flash heating/melting phenomena for crustal rocks at (nearly) seismic slip rates, SCEC Annual Meeting Proceedings and Abstracts, Palm Springs, California.

[8] Kanamori, H., and E. E. Brodsky (2004), The physics of earthquakes, Reports on *Progress in Physics*, 67, 1429 – 1496, doi: 10./1088/0034-4885/67/8/R03.

[9] Kaneko, Y., N. Lapusta, and J.-P. Ampuero (2008), Spectral element modeling of spontaneous earthquake rupture on rate and state faults: Effect of velocity-strengthening friction at shallow depths, *Journal of Geophysical Research*, 113, B09317, doi: 10.1029/2007JB005553.

[10] Kuwano, O., and T. Hatano (2011), Flash weakening is limited by grannular dynamics, *Geophys. Res. Lett.*, 38, L17305, doi:10.1029/2011GL048530.

[11] Liao, Z. (2011), Dynamic strengthening at high-velocity shear experiments, MS thesis, University of Oklahoma, Norman, 54 pp.

[12] Liao, Z., and Z. Reches (2012), Experiment-based model for granite dynamic strength in slip-velocity range of 0.001-1.0 m/s, AGU Annual Meeting, San Francisco, 2012, T13E-2656, ID: 1488537.

[13] Lockner, D. A., and N. M. Beeler (2003), Stress-induced anisotropic poroelasticity response in sandstone, Electronic Proc. 16th ASCE Engin. Mech. Conf., Univ. of Washington, Seattle, WA.

[14] Marone, C. (1998), Laboratory-derived friction laws and their application to seismic faulting, *Annu. Rev. Earth Planet Sci.,* 26, 643-696.

[15] Ohnaka, M., and T. Yamashita (1989) A cohesive zone model for dynamic shear faulting based on experimentally inferred constitutive relation and strong motion source parameters, *Journal of Geophysical Research*, 94 (B4), 4089-4104.

[16] Reches, Z., and D. A. Lockner (2010), Fault weakening and earthquake instability by powder lubrication, *Nature*, 467(7314), 452-455, doi:10.1038/nature09348.

[17] Sammis, C. G., D. A. Lockner, and Z. Reches (2011), The role of adsorbed water on the friction of a layer of submicron particles, *Pure and Applied Geophysics*, doi: 10.1007/s00024-01-0324-0.

http://dx.doi.org/10.5772/54889

[18] Samuelson, J., D. Elsworth, and C. Marone (2009), Shear-induced dilatancy of fluid-saturated faults: experiment and theory, *J. Geophys. Res.*, 114, B12404, doi: 10.1029/2008JB006273.

[19] Schmidt, M., and H. Lipson (2009), Distilling free-form natural laws from experimental data, *Science*, 324, 81-85.

[20] Shimamoto, T., and J. M. Logan (1984), Laboratory friction experiments and natural earthquakes: An argument for long teren tests, *Technophysics*, 109, 165-175.

[21] Tsutsumi, A., and T. Shimamoto (1997), High-velocity frictional properties of gabbro, *Geophys. Res. Lett.*, 24(6), 699-702.